Position and Size Effects On Voids Growth In Nonlinear Elasticity *

Yijiang Lian and Zhiping Li†

LMAM & School of Mathematical Sciences,
Peking University, Beijing 100871, China

Abstract

Numerical studies of multiple voids growth are carried out on a nonlinear hyper-elastic 2D cylinder subjected to an expansionary boundary condition. For certain compressible hyper-elastic material, our numerical experiments on the case of two voids revealed that both the positions and initial sizes of the pre-existing voids can have significant effects on the final grown configuration. We found that, for the initial voids of macroscopic scale both factors affect the final result in a continuous manner and two grown voids of comparable size are commonly observed, and for the initial voids of mesoscopic scale the size effect is no longer continuous and one of the grown voids is always found significantly greater than the other, while for the initial voids of microscopic scale the position effect is essentially decisive on the voids growth and the center positioned void always grows much more rapidly. We also found that the size and position effects are stronger if the material is less compressible, or the load, with the smaller principle stress in alignment with the two voids, is less symmetric.

Keywords and Phrases: position and size effect; void growth; nonlinear elasticity; iso-parametric FEM.

*The research was supported by the NSFC projects 10871011, 11171008 and RFDP of China.
†Corresponding author, email: lizp@math.pku.edu.cn

Contents

1 Introduction

Void growth and cavitation phenomenon has long been considered as a key element in studying fracture mechanism. Early studies focused on the growth of a single void. In 1958, Gent and Lindley [2] had explained the cavitation phenomenon as the dramatic enlargement of small pre-existing voids by analyzing a infinite incompressible elastic shell. Similar studies on elastic-plastic materials can be found in [9, 12]. In 1982, Ball [1] analyzed the radially symmetric solution for a round ball configuration and found that a cavity can also be created in the originally intact body in such a way that the total stored energy of the elastic body can be most efficiently reduced. In 2002, Sivaloganathan [13] had introduced the configurational force to the cavitation, and found that, under certain hypotheses, the center is the unique energetically favorable cavitation point for the standard cavitation problem defined on a round ball [1]. This result together with its theoretical hypotheses has been numerically verified recently by Lian and Li [5].

Because of the obvious great interest both in theory and applications, the problem of the growth and interactions of multiple pre-existing voids has been attracting attentions of researchers in various fields for decades. The problem is relatively better studied by developing cell models for elastic-plastic materials with periodically distributed pre-existing voids. Firstly came the results on the position effect of the voids distribution. In 1972, Needleman [11] analyzed a square array of cylindrical voids. In 1977, Gurson [3] considered a spherical volume with a concentric spherical void. Cylindrical cell models have also been used by Tvergaard [14], [16] in studies of plastic flow localization. The qualitative effect of two size scales of voids was studied in a cell model in 1982 by Tvergaard [15], in which large scale voids are represented by holes with specified size and spacing and small-scale holes are represented by a porous material. In 1996, the size effect was studied by Tvergaard [17] for an elastic-plastic model containing periodically distributed voids of two different sizes. He showed that: for a rather large void volume fraction the voids' interaction leads to relatively more rapid growth of the smaller voids; while in a range of smaller void volume fractions, the trend is opposite; and if the initial void volume fraction is very small, the effect of the voids' interaction dies out and the voids will grow in the same speed.

There are also studies of multiple voids growth and interactions in elastomers (c.f. [10]). More recently, there are some subtle studies on the cavitation criterion and onset-of-cavitation surface of compressible and incompressible hyper-elastic

elastomers under nonsymmetric load [6, 7, 8]. Generally speaking, the numerical study of voids growth with large growth rate for elastic materials is much harder, because the deformation field is much less regular than that of the plastic or elastic-plastic materials, in fact, both the first and second order deformation gradients are singular on the surface of cavities and nearly singular when the voids growth ratio is very large, which is often the case for the growth of very small pre-existing voids. Another difficulty, as was pointed out in [18, 4, 5], is that the standard finite elements such as linear and bilinear conforming finite elements may typically fail to provide an orientation preserving approximation to a large ratio void growth. In 2010, Xu and Henao [18] developed a non-conforming finite element method for the cavitation problem and demonstrated numerical examples of multiple grown voids. In 2011, Lian and Li [5] developed an iso-parametric finite element method and made an initiative study on the size effect for multiple pre-existing macroscopic voids, which basically showed that the growth of a sufficiently large pre-existing void can significantly suppress the growth of other much smaller pre-existing voids. The numerical evidences also indicate that, while the growth of a single pre-existing small void follows a simple principle that it tends to grow bigger if its initial size is increased or it is moved closer toward the center of the ball, the positions and initial sizes of multiple pre-existing voids can interact and compete in a more complicated way.

In the present paper, we will elaborate the sophisticated interacting and competing relationship between the position and size effects for a two voids growth problem defined on a nonlinear compressible hyper-elastic 2D cylinder subjected to an expansionary boundary condition. We will see that, for the initial voids of macroscopic scale both factors affect the final result in a continuous manner and two grown voids of comparable size are commonly observed, and for the initial voids of mesoscopic scale the size effect is no longer continuous and one of the grown voids is always found significantly greater than the other, while for the initial voids of microscopic scale the position effect is essentially decisive on the final grown configuration. We will also see that the size and position effects are stronger if the material is less compressible, or the load, with the smaller principle stress in alignment with the two voids, is less symmetric, and vice versa. It is worth mentioning here that our algorithm, which is based on the quadratic iso-parametric finite element method developed in [5] and a meshing technique adopted in this paper, can successfully compute growth of pre-existing voids as small as 10^{-9} in diameter with the corresponding void growth rate reaching the level of 10^9, and

this, as far as we know, make it possible for the first time to numerical study 2D micro-voids' extremely large growth and interactions in nonlinear elasticity.

The rest of the paper is organized as follows. In section 2, we simply introduce the mathematical model for the voids growth problem. The numerical experiments and results are presented and discussed in section 3. The concluding remarks are made in section 4.

2 Problem Formulation and Discretization

Let $\Omega = \{\boldsymbol{x} : |\boldsymbol{x}| < 1\} \subset \mathbb{R}^2$ being the unit ball in $\mathbb{R}^2$, let $\boldsymbol{x}_i \in \Omega$, $i = 0, \ldots, n$, be $n+1$ distinct given points, and let $1 \gg \varepsilon_i > 0$, $i = 0, \ldots, n$ be given real numbers which satisfy $B_{\varepsilon_i}(\boldsymbol{x}_i) = \{\boldsymbol{x} : |\boldsymbol{x} - \boldsymbol{x}_i| < \varepsilon_i\} \subset \Omega$ and $B_{\varepsilon_i}(\boldsymbol{x}_i) \cap B_{\varepsilon_j}(\boldsymbol{x}_j) = \emptyset$ for all $i, j \in \{0, \ldots, n\}$ and $i \neq j$. Let the stress free reference configuration of an elastic 2D multi-voids cylinder be given by $\Omega_\varepsilon = \Omega \setminus \bigcup_{i=0}^{n} B_{\varepsilon_i}(\boldsymbol{x}_i) \subset \mathbb{R}^2$, where $B_{\varepsilon_i}(\boldsymbol{x}_i) \subset \Omega$, $i = 0, \ldots, n$, are the pre-existing voids of diameters $\varepsilon = \{\varepsilon_i\}_{i=0}^n$ centered at specified points $\{\boldsymbol{x}_i\}_{i=0}^n$.

Denote the initial and current position of material points by $\boldsymbol{x}$ and $\boldsymbol{u}(\boldsymbol{x})$ respectively, and denote the deformation gradient $\nabla \boldsymbol{u}(\boldsymbol{x})$ by $\boldsymbol{F}$. For simplicity, we consider the elastic stored-energy density function $W : M_+^{2\times 2} \to \mathbb{R}$ of the form [13]

$$W(\boldsymbol{F}) = \frac{2}{3}|\boldsymbol{F}|^{\frac{3}{2}} + \frac{\beta}{2}(\det \boldsymbol{F} - 1)^2 + (\det \boldsymbol{F})^{-1}, \tag{1}$$

where $M_+^{2\times 2}$ denotes the real 2×2 matrices with positive determinant and $|\cdot|$ denotes the Euclidean norm ($|\boldsymbol{A}|^2 = \mathrm{trace}(\boldsymbol{A}^{\mathrm{T}}\boldsymbol{A})$), $\beta \in (0, \infty)$ is the bulk modulus which reflect the compressibility of the material. In general the material is less compressible for greater β. The elastic energy density (1) is polyconvex and satisfies

$$\lim_{\det \boldsymbol{F} \to \infty} W(\boldsymbol{F})/\det \boldsymbol{F} = +\infty \quad \text{and} \quad \lim_{\det \boldsymbol{F} \to +0} W(\boldsymbol{F}) = +\infty,$$

which are the important features shared by many elastomer materials. The stress of the material at deformation gradient ∇u can be calculated by

$$D_F W(\nabla \boldsymbol{u}) = \left|\nabla \boldsymbol{u}\right|^{-1/2} \nabla \boldsymbol{u} + \left(\beta(\det \nabla \boldsymbol{u} - 1) - (\det \nabla \boldsymbol{u})^{-2}\right) \mathrm{adj}\, \nabla \boldsymbol{u}^{\mathrm{T}}, \tag{2}$$

where $\mathrm{adj}\, \boldsymbol{A}$ is the adjoint matrix of $\boldsymbol{A}$. To better understand the mechanical response of the material when thin wall structure forms between grown voids, we show in Figure 1(a) and 1(b) the stress-strain relationship of the material with

the bulk modulus $\beta = 1$ and for special deformations with diagonal deformation gradients $\nabla u = \mathrm{diag}(d/u_{22}, u_{22})$, where $\sigma_{ij} \equiv (D_F W(\nabla \boldsymbol{u}))_{ij}$ and $u_{ij} \equiv \partial_j u_i$. In particular we have that, for u_{22} sufficiently large, when $d = \det \nabla \boldsymbol{u} \approx$ the root of $\beta d^3 - \beta d^2 - 1 = 0$ (≈ 1.5 if $\beta = 1$, and ≈ 1.1 if $\beta = 10$), the material is approximately subject to uniaxial tension, which is the case on the surface of a grown void where tension free boundary condition is proposed.

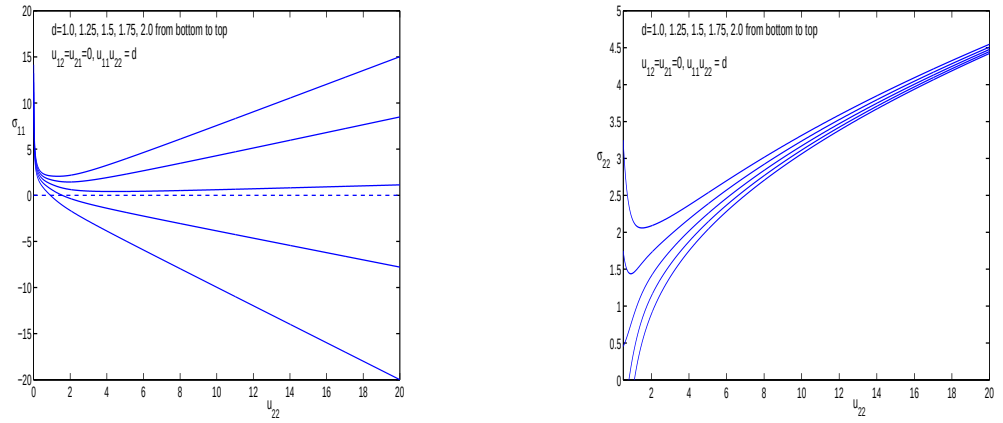

(a) $\sigma_{11} \approx 0$ for $d \approx 1.5$ and $u_{22} \gg 1$.

(b) σ_{22} is strictly increasing for $u_{22} > d$.

Figure 1: Stress-strain relations of the material in special uniaxial cases.

The specific problem we consider is to minimize the total elastic energy

$$E(\boldsymbol{u}) = \int_{\Omega_\varepsilon} W(\nabla \boldsymbol{u}(\boldsymbol{x}))d\boldsymbol{x} \tag{3}$$

in a set of admissible deformations

$$\mathbb{U} = \left\{ \boldsymbol{u} \in W^{1,1}(\Omega_\varepsilon; \mathbb{R}^2) \text{ is a bijection} : \boldsymbol{u}|_{\Gamma_0} = \lambda \boldsymbol{x}, \ \det \nabla \boldsymbol{u} > 0 \ \text{ a.e.} \right\}, \tag{4}$$

where $\Gamma_0 = \partial\Omega = \{\boldsymbol{x} : |\boldsymbol{x}| = 1\}$ is the expansionary boundary and $\lambda > 1$ is the expansion rate.

The corresponding mixed displacement/traction boundary value problem of the Euler-Lagrange equation is :

$$\mathrm{div}(D_F W(\nabla \boldsymbol{u})) = \boldsymbol{0}, \qquad \text{in } \Omega_\varepsilon, \tag{5}$$

$$D_F W(\nabla \boldsymbol{u})\, \boldsymbol{\nu} = \boldsymbol{0}, \qquad \text{on } \cup_{i=0}^{n} \Gamma_i, \tag{6}$$

$$\boldsymbol{u}(\boldsymbol{x}) = \lambda \boldsymbol{x}, \qquad \text{on } \Gamma_0, \tag{7}$$

where $\boldsymbol{\nu}$ denotes the unit exterior normal with respect to Ω_ε, $\Gamma_i = \partial B_{\varepsilon_i}(\boldsymbol{x}_i)$, $i = 0, \cdots, n$, are the boundaries of the pre-existing voids.

One of the key element we use to numerically solving the Euler-Lagrange equation (5) is to combine the quadratic iso-parametric finite element discretization [5] with a properly designed meshing technique. This is inspired by the fact that a mesh, which is locally radially symmetric around each small pre-existing void and consists of curved triangular elements established according to the corresponding local polar coordinates of each void, plays a crucial role in accommodating locally large expansion dominant deformations [4, 5]. In our numerical experiments, we synthesized an Easymesh produced mesh and a locally radially symmetric mesh [4] around each pre-existing void to obtain a cavitation accommodating mesh with quadratic triangular elements on Ω_ε in the following way:

- First, we use the Easymesh to produce a mesh $\mathcal{J}'$ on $\Omega_{\hat{\varepsilon}}$ with relatively larger voids. Then, we transform the straight sided triangular elements close to $\cup_0^n \Gamma_i$ into quadratically curved ones according to the corresponding polar coordinates of Γ_i, $i = 0, 1, \ldots, n$ [5]. Figure 2(a) illustrates an example of such a mesh with $\boldsymbol{x}_0 = (0.0, 0.0)$, $\boldsymbol{x}_1 = (0.3, 0.0)$ and $\hat{\varepsilon}_0 = \hat{\varepsilon}_1 = 0.1$.

- Next, we introduce a few layers of locally radially symmetric mesh $\mathcal{J}_i$ with quadratically curved triangular elements consistent with the local polar coordinates on the circular ring region $\{\boldsymbol{x} : \varepsilon_i \leq |\boldsymbol{x} - \boldsymbol{x}_i| \leq \hat{\varepsilon}_i\}$ around the ith void, $i = 1, \cdots, n$.

- The final mesh is defined as $\mathcal{J} = \mathcal{J}' \bigcup (\bigcup_{i=0}^{n} \mathcal{J}_i)$. Figure 2(b) shows an example, which has two layers of local polar coordinates consistent quadratic mesh added for each void.

We remark here that, when the growth ratio is very large, which is typical if the pre-existing void is small, the above technique is necessary for our algorithm to guarantee that, on a mesh with reasonably many degrees of freedom, the obtained deformation $\boldsymbol{u}$ is orientation preserving, or equivalently $\det \nabla \boldsymbol{u} > 0$, which is a very important physical requirement yet is often ignored by many researchers in the computation of voids' growth. Recently, it is shown in [18] that the linear finite element method (in fact any straight sided finite element method) is computationally impractical to achieve the orientation preserving property in the neighborhood of voids with very large growth ratio.

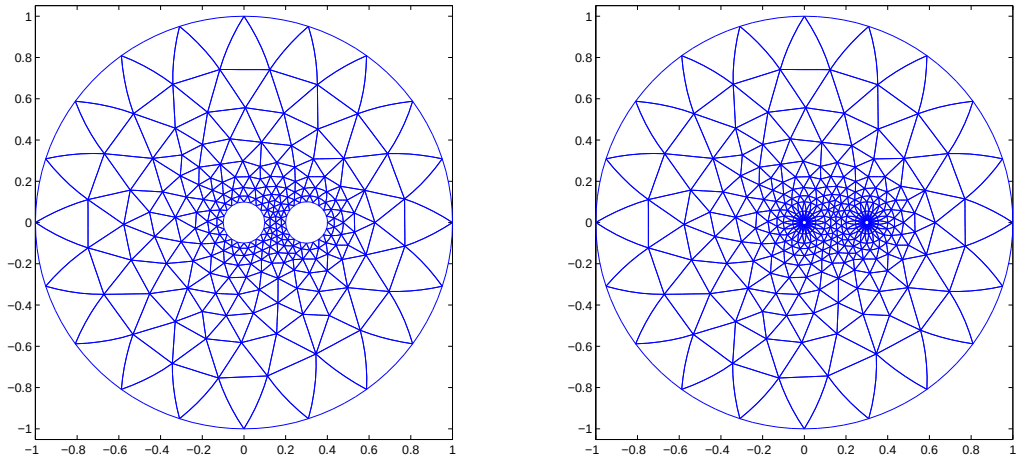

(a) A mesh $\mathcal{J}'$ produce by Easymesh. (b) The final mesh $\mathcal{J}$.

Figure 2: A cavitation accommodating mesh for two voids.

3 Numerical Experiments and Results

We focus on the case of two pre-existing voids. In most of our numerical experiments, we consider radially symmetric expansion with expansion rate $\lambda = 2$, and the bulk modulus is set to $\beta = 1$. First, we will investigate the pure position effect in Section 3.1 by considering two pre-existing voids of equal size. Then, we will study in Section 3.2 the pure size effect by positioning the two pre-existing voids symmetrically with respect to the origin. In Section 3.3, we will see how the position and size effects compete in the voids' growth on different initial size scales of the pre-existing voids. Some typical evolution processes of voids' growth and interactions are shown in Section 3.4. The effect of compressibility and loss of radial symmetry of the expansion will be examined in Section 3.5.

3.1 Pure Position Effect

Let $\boldsymbol{x}_0 = (-0.4, 0)$, $\boldsymbol{x}_1 = (z, 0)$, $\varepsilon_0 = \varepsilon_1 = 0.01$. Some typical numerical results are illustrated in Figure 3. Our numerical experiments show that, if $|z| > 0.4$ the void 0 grows faster, otherwise the void 1 grows faster, and in particular, if $z \in (-0.4, 0]$ the grown void 1 can overwhelmingly dominate the final configuration as shown in Figure 3(a) and Figure 4(a), where v_i represents the final volume of the grown void i, $i = 0, 1$.

The numerical results indicate that, while the void closer to the center of the ball, which is the energetically most favorable cavitation point, tends to grow faster,

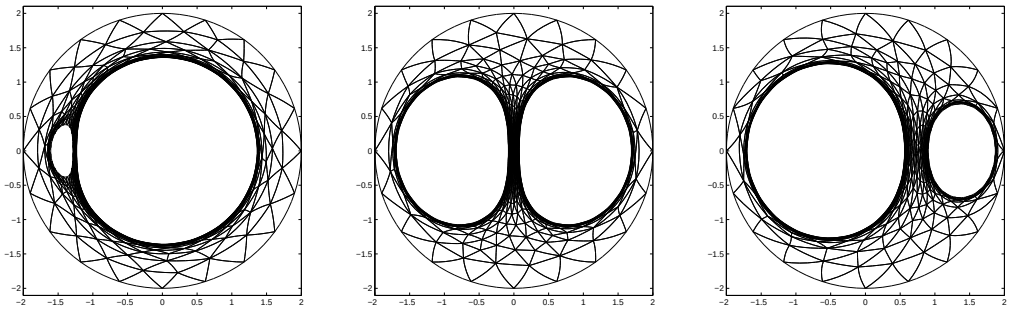

(a) $\boldsymbol{x}_1 = (0.0, 0)$. (b) $\boldsymbol{x}_1 = (0.4, 0)$. (c) $\boldsymbol{x}_1 = (0.69, 0)$.

Figure 3: Pure position effect for two pre-existing voids with $\boldsymbol{x}_0 = (-0.4, 0)$.

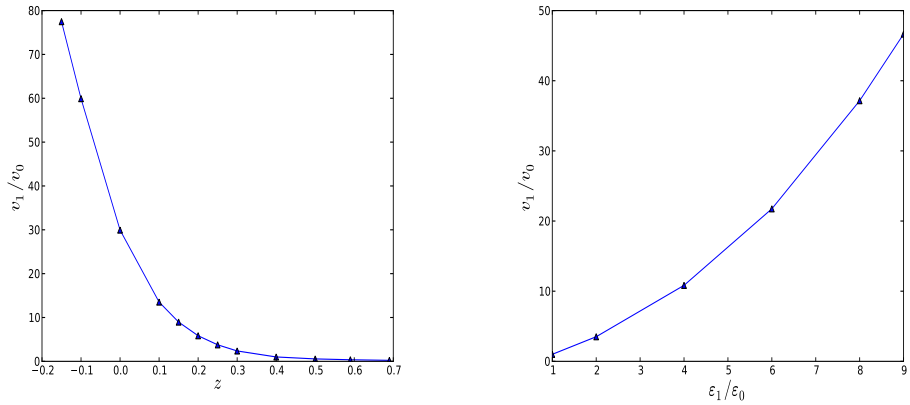

(a) Pure position effect. (b) Pure size effect.

Figure 4: Pure position and size effects on the final volumes' ratio.

it is the relative position that dramatically affects the final configuration. In fact, the numerical experiments show that the growth of the void positioned at an energetically less favorable cavitation point will be more severely suppressed if it is approached by the other void from the energetically more favorable direction. In other words, the interaction between the two voids is always in favor of the one closer to the center of the ball, and the final volume ratio of the two grown voids is getting increasingly greater as the initial distance between the two pre-existing voids is decreased.

3.2 Pure Size Effect

Let $\boldsymbol{x}_0 = (-0.4, 0)$, $\boldsymbol{x}_1 = (0.4, 0)$, and $\varepsilon_0 = 0.01$, we will see how the size ε_1 affect the growth of the two symmetrically positioned pre-existing voids. Some

typical numerical results on the final configuration are illustrated in Figure 5. Our numerical experiments show that, for symmetrically positioned two pre-existing voids, the relatively greater initial size leads to faster growth of the corresponding void. In fact, as is shown in Figure 4(b), the final volume ratio v_1/v_0 of the two grown voids is a super linear increasing function of the initial size ratio $\varepsilon_1/\varepsilon_0$.

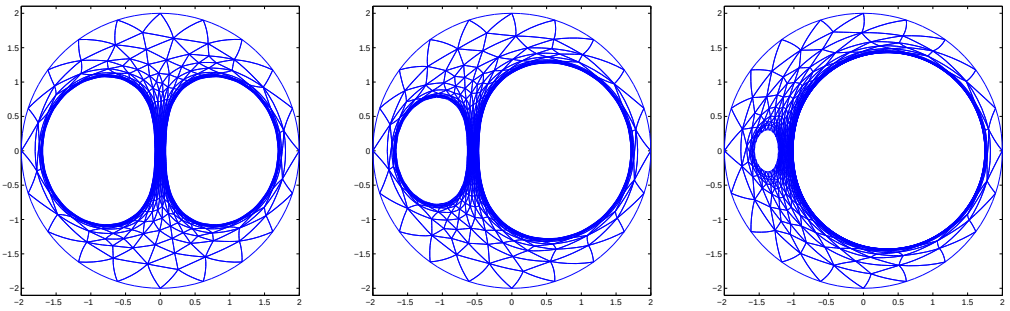

(a) $\varepsilon_1 = 0.01$. (b) $\varepsilon_1 = 0.02$. (c) $\varepsilon_1 = 0.08$.

Figure 5: Pure size effect for $\boldsymbol{x}_0 = (-0.4, 0)$, $\boldsymbol{x}_1 = (0.4, 0)$, $\varepsilon_0 = 0.01$.

3.3 Position vs Size, from Macro to Micro Scales

In this subsection, we elaborate the competitive relationship between the position and size effect on different size scales. We use the terms macro, meso and micro for different length scales appeared in the numerical experiments, which do not necessarily represent the real physical length scales. For simplicity, we set $\boldsymbol{x}_0 = (0, 0)$ and $\boldsymbol{x}_1 = (z, 0)$. However, the phenomenon revealed by the numerical experiments can generally be observed if $|\boldsymbol{x}_0| < |\boldsymbol{x}_1|$ and $|\boldsymbol{x}_0| \ll |\boldsymbol{x}_1 - \boldsymbol{x}_0|$.

We start with the macroscopic scale when $0.1 \geq \varepsilon_i \geq 0.04$, $i = 0, 1$. Some typical numerical results for the case of macroscopic scale are illustrated in Figure 6(a) and Figure 7(a). Our numerical experiments show that, in the macroscopic case, the volumes of the two grown voids are generally comparable and depend continuously on the positions and initial sizes of the pre-existing voids, and the volume ratio v_1/v_0 is approximately a cubic function of the size ratio $\varepsilon_1/\varepsilon_0$.

Next, we consider the mesoscopic scale when $10^{-4} \leq \varepsilon_0 \leq 10^{-2}$. Some typical numerical results for the case of mesoscopic scale are illustrated in Figure 6(b), Figure 6(c) and Figure 7(b). Our numerical experiments show that, in the mesoscopic

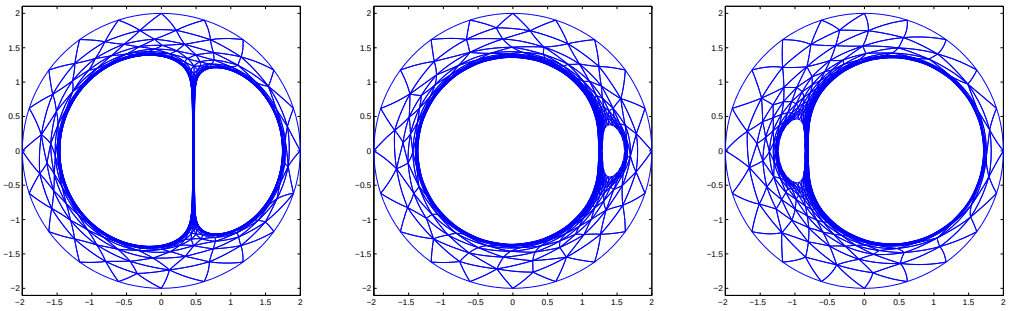

(a) $\varepsilon_0 = 0.1, \varepsilon_1 = 0.1$ (b) $\varepsilon_0 = 0.01, \varepsilon_1 = 0.01$ (c) $\varepsilon_0 = 0.01, \varepsilon_1 = 0.02$

Figure 6: The grown voids with typical initial sizes ($z = 0.4$).

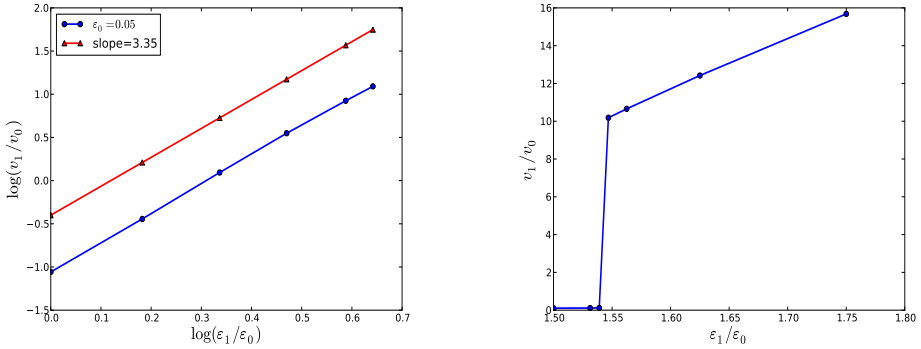

(a) Macroscopic scale, $\varepsilon_0 = 0.05$. (b) Mesoscopic scale, $\varepsilon_0 = 0.01$.

Figure 7: Typical size effects on different scales ($z = 0.4$).

case, there exists a critical size $\varepsilon_1^{cri}(\varepsilon_0, z)$ such that

$$\frac{v_1}{v_0} \begin{cases} \gg 1, & \text{if } \varepsilon_1 > \varepsilon_1^{cri}; \\ \ll 1, & \text{if } \varepsilon_1 < \varepsilon_1^{cri}, \end{cases} \tag{8}$$

and (see Table 1)

$$\frac{v_1 \varepsilon_0^2}{v_0 \varepsilon_1^2} \begin{cases} > 1, & \text{if } \varepsilon_1 > \varepsilon_1^{cri}; \\ < 1, & \text{if } \varepsilon_1 < \varepsilon_1^{cri}, \end{cases} \tag{9}$$

In other words, on mesoscopic scale, the volume ratio v_1/v_0 is no longer a continuous function on the size ratio $\varepsilon_1/\varepsilon_0$, although there might still be two observable grown voids, one of them is always much bigger than the other (see (8)), and we see in (9) that, if $\varepsilon_1 < \varepsilon_1^{cri}$, the growth is in favor of the pre-existing void closer to the center of the ball, and the size effect takes in dominant charge only when $\varepsilon_1 > \varepsilon_1^{cri}$. In fact, one can generally observe a sharp switch from a centric dominant solution as shown

in Figure 6(b) to an eccentric dominant solution as shown in Figure 6(c) when ε_1 increasingly passes the critical value ε_1^{cri}. This is in contrast to the continuous change in the macroscopic case (see Figure 8(a) for a comparison).

Last but not least, we consider the case of microscopic case when $\varepsilon_0 \leq 10^{-4}$. Our numerical experiments show that, similar as the mesoscopic case, there exists a critical size $\varepsilon_1^{cri}(\varepsilon_0, z)$ such that (see Figure 8(b))

$$\frac{v_1}{v_0} \begin{cases} \gg 1, & \text{if } \varepsilon_1 > \varepsilon_1^{cri}; \\ \ll 1, & \text{if } \varepsilon_1 < \varepsilon_1^{cri}, \end{cases} \tag{10}$$

however, in microscopic case, the growth is always in favor of the pre-existing void closer to the center of the ball (see Table 1), that is

$$v_1 \varepsilon_0^2 < v_0 \varepsilon_1^2, \qquad \forall \varepsilon_1. \tag{11}$$

ε_0	$\frac{v_1\varepsilon_0^2}{v_0\varepsilon_1^2}$ $(\varepsilon_1 \nearrow \varepsilon_1^{cri})$	$\frac{v_1\varepsilon_0^2}{v_0\varepsilon_1^2}$ $(\varepsilon_1 \searrow \varepsilon_1^{cri})$
1.0e-02	3.3986e-02	4.8414e+00
1.0e-03	9.9515e-04	7.7094e+00
1.0e-04	1.4906e-05	1.4584e-01
1.0e-05	1.5485e-07	2.3003e-03
1.0e-06	1.5259e-09	2.2172e-05

Table 1: The ratio of the growth speed of the two voids across ε_1^{cri} $(z = 0.4)$.

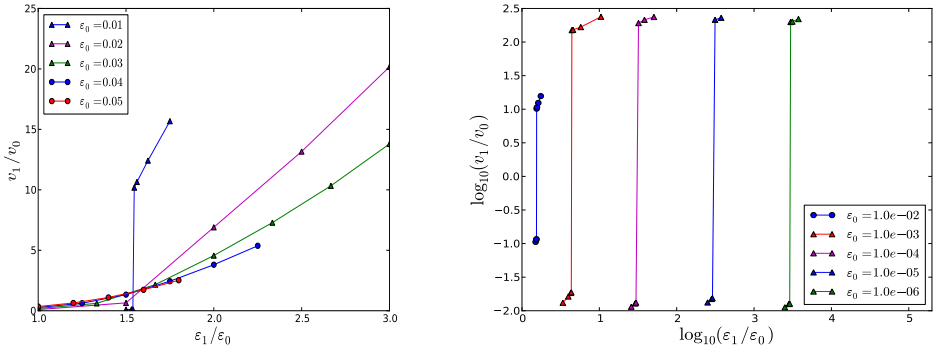

(a) From Macro to Meso.

(b) From Meso to Micro.

Figure 8: The behavior of v_1/v_0 as a function of $\varepsilon_1/\varepsilon_0$ for various ε_0 $(z = 0.4)$.

Our numerical experiments also show that the critical size $\varepsilon_1^{cri}(\varepsilon_0, z)$ is a continuous function and is a monotonically increasing function for both variables (see

Figure 9(a) and Figure 9(b)). Figure 9(a) shows $\varepsilon_1^{cri}(\varepsilon_0, \cdot)$ as functions of z for various fixed ε_0, where we see that, for $\varepsilon_0 \leq 10^{-4}$, $\varepsilon_1^{cri}(\varepsilon_0, \cdot)$ is almost independent of ε_0. More precisely, we see in Figure 9(b) that,

$$\lim_{\varepsilon_0 \to 0} \varepsilon_1^{cri}(\varepsilon_0, z) = \varepsilon_1^{cri}(\infty, z) > 10^{-3}, \qquad \text{if } \ z \geq 0.3. \tag{12}$$

This indicates, in particular, if both of the pre-existing voids are sufficiently small, only the centric dominant solution can be observed.

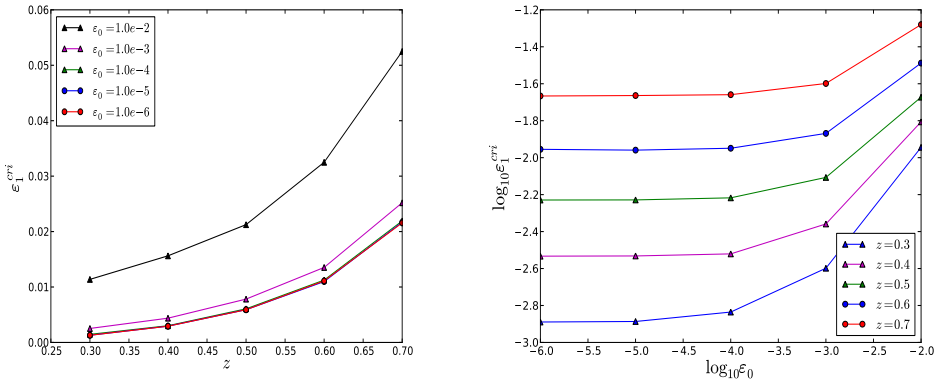

(a) $\varepsilon_1^{cri}(\varepsilon_0, z)$ as a function of z. (b) $\varepsilon_1^{cri}(\varepsilon_0, z)$ as a function of ε_0.

Figure 9: $\varepsilon_1^{cri}(\varepsilon_0, z)$ as a function of ε_0 and z.

3.4 Evolution Process of Voids' Growth and Interactions

Even though the problem we solve is a static one, our iterative scheme is essentially based on a weighted gradient flow [5], which follows a quasi-static path leading to the equilibrium of the system. Hence, the iteration process, which approximately traces the quasi-static evolution process of the voids' growth and interactions, could help us to better understand the numerical solution and corresponding physical process. In presenting the numerical results of the iteration process, we chose to omit the possibly oscillatory initial steps which are far away from a quasi static path, and focus on the behavior of the process when it is approaching an equilibrium.

Figure 10 illustrates the evolution process of the formation of the thin wall structure in the macroscopic case shown in Figure 6(a). In Figure 10(a), the final (yet representative during the iteration process) mesh distribution on a middle part of the thin wall is displayed, where we see that the deformed mesh is severely stretched in one direction and compressed in another, but otherwise quite regularly

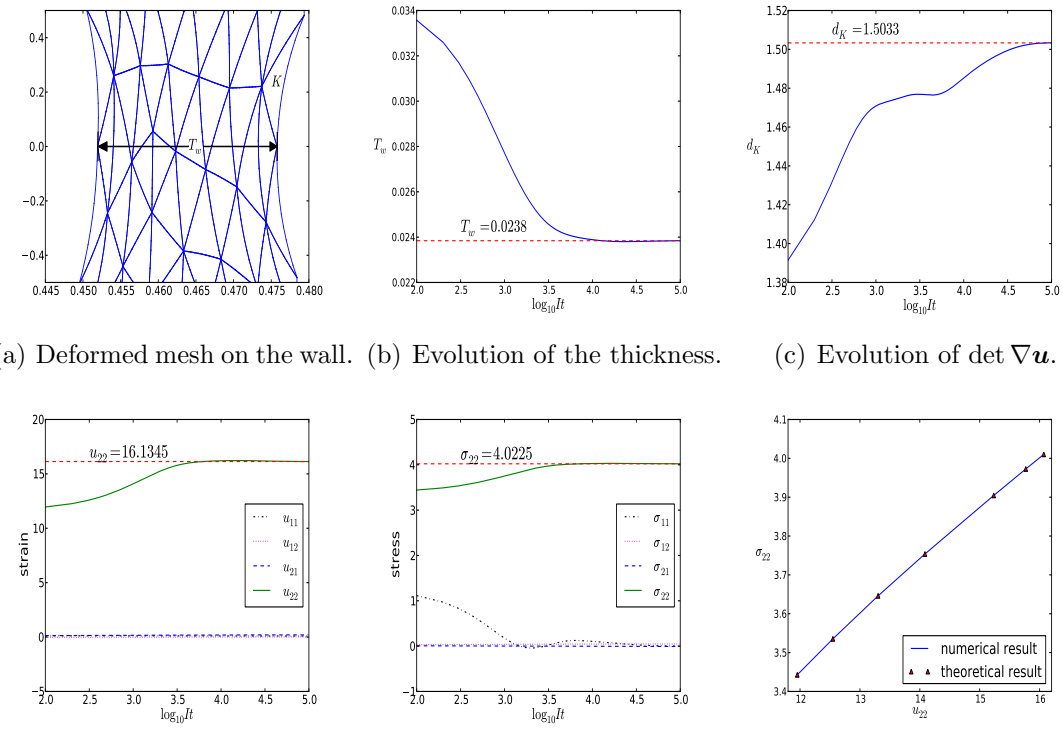

(a) Deformed mesh on the wall. (b) Evolution of the thickness. (c) Evolution of $\det \nabla \boldsymbol{u}$.

(d) Evolution of $\nabla \boldsymbol{u}$. (e) Evolution of $D_F W(\nabla \boldsymbol{u})$. (f) Stress-strain relation.

Figure 10: The evolution process of a typical thin wall structure.

distributed on the thin wall. Figure 10(b) shows the evolution and convergence behavior of the thickness T_w of the thin wall, where It is the number of iterations. Figure 10(c) shows the evolution process of the determinant of the average deformation gradient $d_K = \det \nabla \boldsymbol{u}|_K$ on a typical element (marked by K in Figure 10(a)), we see that d_K converges to a value close to 1.5 as expected. Figure 10(d) and 10(e) show the evolution process of the corresponding strain and stress on the element K, and the final state is obviously close to a uniaxial tensile case. Figure 10(f) demonstrates the path of the stress-strain relation during the evolution process, where the numerical result follows the iteration process and the theoretical result is calculated by setting in the formula (2) $\nabla \boldsymbol{u} = \mathrm{diag}(d_K/u_{22}, u_{22})$ with d_K taking values at corresponding iterations.

Figure 11(a) and 11(b) show typical evolution processes of the growing volumes of pre-existing voids in macroscopic and mesoscopic scales respectively, while Figure 11(c) and 11(d) demonstrate the evolution processes of the corresponding volume ratios v_1/v_0. We see in Figure 11(a) and Figure 11(b) that the evolution process can be divided into two stages. At the initial stage of evolution, the two

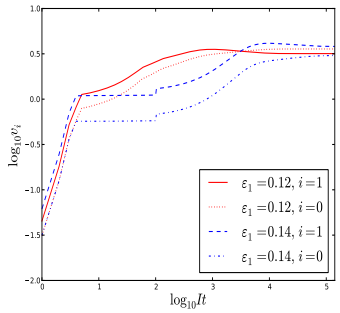

(a) Macroscopic scale ($\varepsilon_0 = 0.1$)

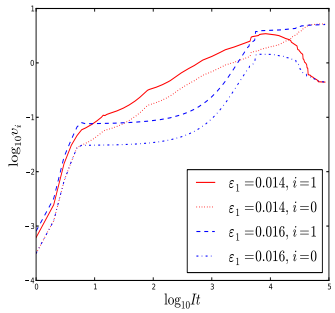

(b) Mesoscopic scale ($\varepsilon_0 = 0.01$)

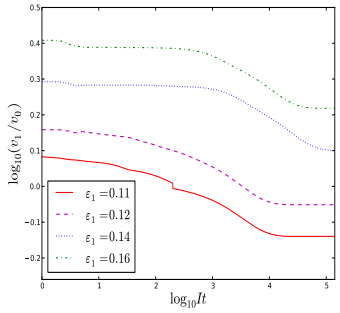

(c) Macroscopic scale ($\varepsilon_0 = 0.1$)

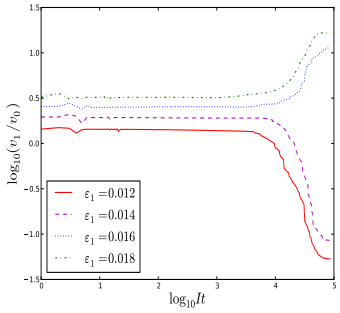

(d) Mesoscopic scale ($\varepsilon_0 = 0.01$)

Figure 11: Typical evolution processes of v_0, v_1 and v_1/v_0.

pre-existing voids grow pretty much independently at almost the same speed. The nearly independent growth stage continues until the volumes reach certain level, then the interaction between the two growing voids starts to play an obvious and decisive role. At the interaction stage, one of the void is forced to grow in much slower speed (see Figure 11(a)), and even start to shrink rapidly (see Figure 11(b)). The interaction stage can also be characterized by the rapid change of the volume fractions (see Figure 11(c) and 11(d)).

3.5 Effect of Compressibility and Unsymmetry of Load

As shown in [6, 7, 8], the material compressibility and unsymmetry of load play interesting roles in defect growth and onset-of-cavitation surfaces in elastomeric solids. We expect that they will also affect the interactions between the growing voids, and thus affect somehow the size and position effects. An intuitive observation suggests that, as the material becomes less compressible, the thin wall structure between the two growing voids must become thinner to cope with the

drop of volume increase on the surfaces of grown voids (see Section 2), hence the interactions between fast growing voids must become stronger and thus sharpened the size and position effects. Our numerical experiments show that this is indeed the case. On the other hand, the effect of unsymmetry of load is more subtle, our numerical experiments show that the unsymmetry of load can weaken or strengthen the interactions between the grown voids if the load is applied in different directions with respect to the two voids.

Figure 12 show some typical numerical results of pure size effect with the expansion rate $\lambda = 2$ and bulk modulus $\beta = 9$ (compared with Figure 5 where $\beta = 1$). Figure 13(a) and 13(b) show how the volume ratios of pure size and pure position effects are affected when the bulk modulus β varies. It is clearly seen that, in either case, the final voids' ratio v_1/v_0 tends to change faster for greater β.

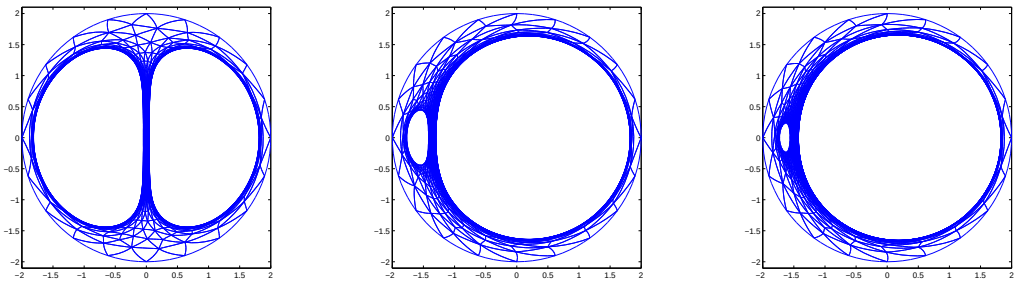

(a) $\varepsilon_1 = 0.01$. (b) $\varepsilon_1 = 0.02$. (c) $\varepsilon_1 = 0.08$.

Figure 12: The size effect for $\boldsymbol{x}_0 = (-0.4, 0)$, $\boldsymbol{x}_1 = (0.4, 0)$, $\varepsilon_0 = 0.01$, $\beta = 9.0$.

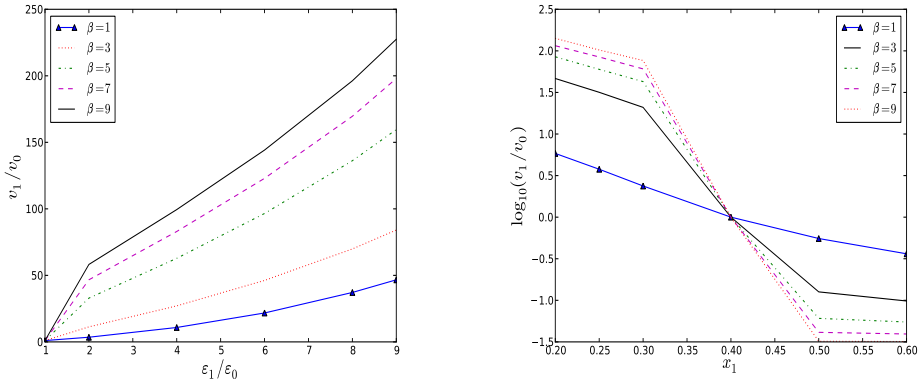

(a) Pure size effect. (b) Pure position effect.

Figure 13: The influence of bulk modulus on the position and size effects.

Figure 14 show the size effect on different scales for various bulk modulus β (see also Figure 7(b) for $\beta = 1$). We see that the critical size $\varepsilon_1^{cri}(\varepsilon_0, z, \beta)$ (here $\varepsilon_0 = 0.01$, $z = 0.4$) is a decreasing function of the bulk modulus β, and we have $\varepsilon_1^{cri}(0.01, 0.4, \beta) \approx \varepsilon_1^{cri}(0.01, 0.4, 5) \approx 0.0135$ for all $\beta \geq 5$.

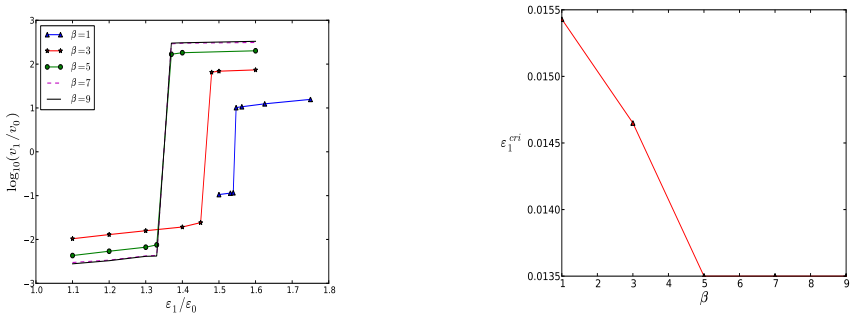

Figure 14: The size effect with $\varepsilon_0 = 0.01$ and $z = 0.4$ for various β.

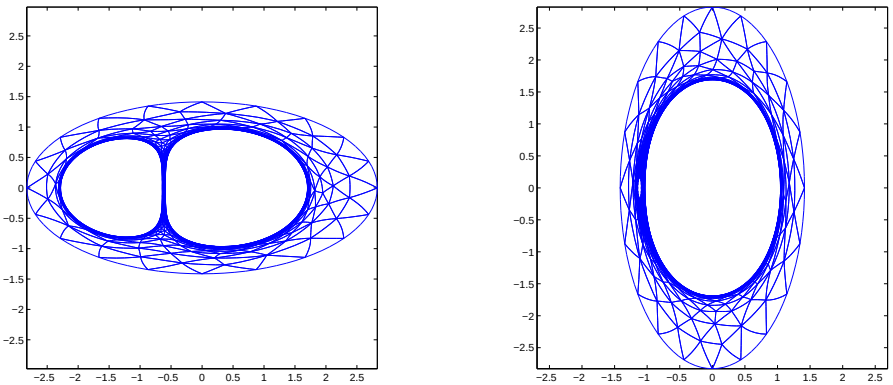

(a) $\lambda_h = 2\sqrt{2}, \lambda_v = \sqrt{2}, \beta = 1$.

(b) $\lambda_h = \sqrt{2}, \lambda_v = 2\sqrt{2}, \beta = 1$.

(c) $\lambda_h = 2.2, \lambda_v = 1.8182, \beta = 1$.

(d) $\lambda_h = 1.8182, \lambda_v = 2.2, \beta = 1$.

Figure 15: The position effect for $\boldsymbol{x}_0 = (-0.4, 0)$, $\boldsymbol{x}_1 = (0.0, 0)$, $\varepsilon_0 = \varepsilon_1 = 0.01$.

Figure 15 and 16 show some typical numerical results of the position and size effects for two horizontally aligned voids' growth under ellipse shaped expansion boundary conditions, where λ_h and λ_v are the horizontal and vertical expansion rates along the two principle axes respectively. For the sake of comparison with the symmetric case (see Figure 3(a) and 5(b)), λ_h and λ_v are set to satisfy $\lambda_h\lambda_v = 4$, and β is set to 1. It is seen that, both the position and the size effects are clearly weakened if the two voids are aligned with the long axis of the ellipse, while it is obviously strengthened if the alignment axis is the short one.

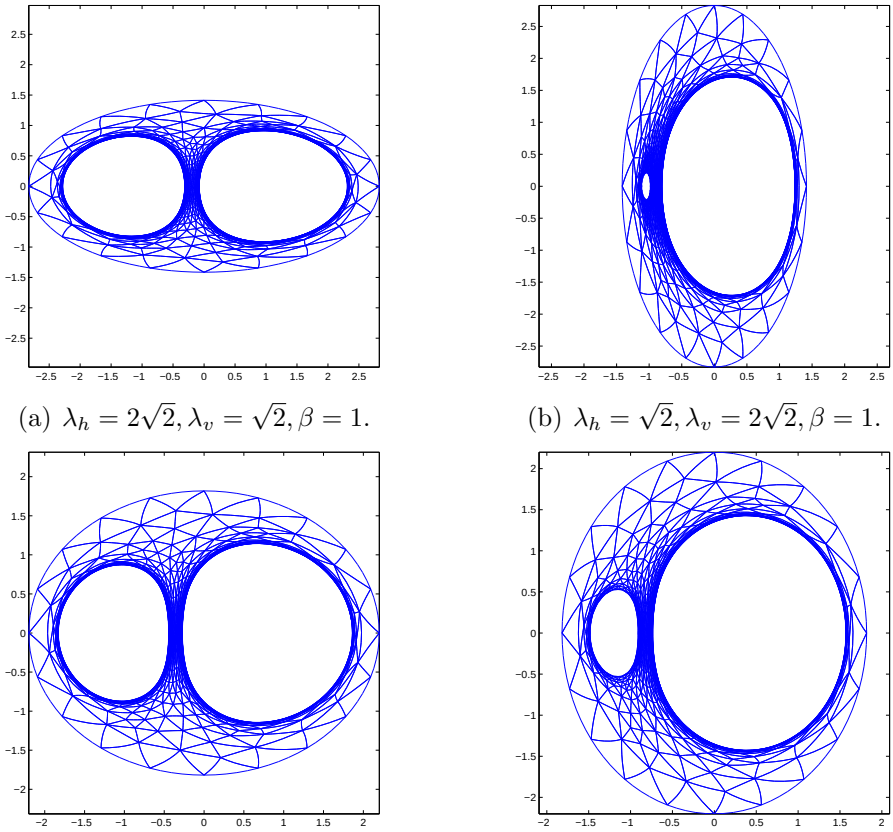

(a) $\lambda_h = 2\sqrt{2}, \lambda_v = \sqrt{2}, \beta = 1.$ (b) $\lambda_h = \sqrt{2}, \lambda_v = 2\sqrt{2}, \beta = 1.$

(c) $\lambda_h = 2.2, \lambda_v = 1.8182, \beta = 1.$ (d) $\lambda_h = 1.8182, \lambda_v = 2.2, \beta = 1.$

Figure 16: The size effect for $\boldsymbol{x}_0 = (-0.4, 0)$, $\boldsymbol{x}_1 = (0.4, 0)$, $\varepsilon_0 = 0.01, \varepsilon_1 = 0.02$.

4 Summary

For a void growth problem defined on a 2D nonlinear hyper-elastic ball, which has two pre-existing voids and is subjected to an expansionary boundary condition, it is found that both the positions $\boldsymbol{x}_0$, $\boldsymbol{x}_1$ and sizes ε_0, ε_1 of the two pre-existing

voids, namely void 0 and void 1, have significant impact on the final configuration. Our numerical experiments indicate that, for fixed positions, the size effect can be classified into three length scales, which are termed as macroscopic, mesoscopic and microscopic scales. The numerical results are summarized as follows.

In the macroscopic scale, when both of the voids are big, the two voids will grow in comparable speed, and the volume ratio of the grown voids depend continuously on the positions and sizes of the two pre-existing voids. In this case, there are always two grown voids of comparable size in the final configuration.

However, when the void much closer to the center of the ball is sufficiently small, the dependence of the growth speed and volume ratio on the initial positions and sizes are no longer continuous, and one of the grown void will have much greater volume than the other in the final configuration. This includes the mesoscopic and microscopic cases, when we assume that $|\boldsymbol{x}_0| < |\boldsymbol{x}_1|$ and $|\boldsymbol{x}_0| \ll |\boldsymbol{x}_1 - \boldsymbol{x}_0|$.

In the microscopic scale, when ε_0 is very small, the void 0, which is much closer to the center of the ball, will always grow in faster speed, and there exists a critical size $\varepsilon_1^{cri}(\varepsilon_0, \boldsymbol{x}_0, \boldsymbol{x}_1)$, which is usually much greater than ε_0, such that, if ε_1 is less than the critical size, then the final configuration will be dominated by the void 0, and vice vera. In particular, if the two pre-existing voids are both very small, then the final configuration will be dominated by the grown void 0.

In the mesoscopic scale, when ε_0 is somewhere between the macroscopic and microscopic scales, there exists a critical size $\varepsilon_1^{cri}(\varepsilon_0, \boldsymbol{x}_0, \boldsymbol{x}_1)$, which is greater than but usually in the same order as ε_0, such that, if ε_1 is less than the critical size, then the void 0 will grow faster and the final configuration is dominated by the grown void 0, and vice vera.

As the initial size of the pre-existing void decreases from the macroscopic scale to the microscopic scale, the tensile strain level on the surface of the grown void increases sharply. In particular, we see that, in the microscopic scale, the tensile strain level on the surface of the grown void 0 is always much higher than that of the grown void 1. Thus, in the growing process, it is more likely that the corresponding stress on the growing void 0 will first exceed whatever fracture criterion of a practical elastic material.

The size and position effects are obviously sharpened as the bulk modulus β increases. The effect of unsymmetry of load is more subtle. Our numerical experiments show that the size and position effects are weakened if the greater principle stress is aligned with the two voids, and the effects are strengthened if the smaller principle stress is the axis of alignment.

Acknowledgment: The research was supported by the NSFC projects 10871011, 11171008 and RFDP of China. The AFEPack is used in our computation for the implement of the isoparametric finite element, we are grateful to Professor Ruo Li of Peking University to help us on the use of the powerful software. We would also like to thank the reviewers for their valuable comments and suggestions, which helped greatly in improving the quality of our paper.

References

[1] J. M. Ball. Discontinuous equilibrium solutions and cavitation in nonlinear elasticity. *Philosophical Transactions of the Royal Society of London. Series A, Mathematical and Physical Sciences*, 306:557–611, 1982.

[2] A. N. Gent and P. B. Lindley. International rupture of bonded rubber cylinders in tensions. *Proceedings of the Royal Society. Series A*, 249:195–205, 1958.

[3] A. L. Gurson. Continuum theory of ductile rupture by void nucleation and growth: Part i—yield criteria and flow rules for porous ductile media. *Journal of Engineering Materials and Technology*, 99(1):2–15, 1977.

[4] Yijiang Lian and Zhiping Li. A dual-parametric finite element method for cavitation in nonlinear elasticity. *Journal of Computational and Applied Mathematics, doi: 10.1016/j.cam.2011.05.020*, 2011.

[5] Yijiang Lian and Zhiping Li. A numerical study on cavitations in nonlinear elasticity - defects and configurational forces. *Mathematical Models and Methods in Applied Sciences, doi: 10.1142/S0218202511005830*, 2011.

[6] Oscar Lopez-Pamies. Onset of cavitation in compressible, isotropic, hyperelastic solids. *Journal of Elasticity*, 94:115–145, 2009.

[7] Oscar Lopez-Pamies, Toshio Nakamura, and Martin I. Idiart. Cavitation in elastomeric solids: I—a defect-growth theory. *Journal of the Mechanics and Physics of Solids*, 59:1464–1487, 2011.

[8] Oscar Lopez-Pamies, Toshio Nakamura, and Martin I. Idiart. Cavitation in elastomeric solids: II—onset-of-cavitation surfaces for neo-hookean materials. *Journal of the Mechanics and Physics of Solids*, 59:1488–1505, 2011.

[9] F.A. McClintock. A criterion for ductile fracture by growth of holes. *Journal of Applied Mechanics*, 41:964–970, 1968.

[10] J.C. Michel, O. Lopez-Pamies, P. Ponte Castañeda, and N. Triantafyllidis. Microscopic and macroscopic instabilities in finitely strained porous elastomers. *Journal of the Mechanics and Physics of Solids*, 55:900–938, 2007.

[11] A. Needleman. Void growth in an elastic-plastic medium. *Journal of Applied Mechanics*, 39(4):964–970, 1972.

[12] J. R. Rice and D. M. Tracey. On the ductile enlargement of voids in triaxial stress fields. *Journal of the Mechanics and Physics of Solids*, 17:201 – 217, 1969.

[13] Jeyabal Sivaloganathan and Scott J. Spector. On cavitation, configurational forces and implications for fracture in a nonlinearly elastic material. *Journal of Elasticity*, 67:25–49, 2002.

[14] Viggo Tvergaard. Influence of voids on shear band instabilities under plane strain conditions. *International Journal of Fracture*, 17:389–407, 1981.

[15] Viggo Tvergaard. Ductile fracture by cavity nucleation between larger voids. *Journal of the Mechanics and Physics of Solids*, 30:265 – 286, 1982.

[16] Viggo Tvergaard. On localization in ductile materials containing spherical voids. *International Journal of Fracture*, 18:237–252, 1982.

[17] Viggo Tvergaard. Effect of void size difference on growth and cavitation instabilities. *Journal of the Mechanics and Physics of Solids*, 44(8):1237 – 1253, 1996.

[18] Xianmin Xu and Duvan Henao. An efficient numerical method for cavitation in nonlinear elasticity. *Mathematical Models and Methods in Applied Sciences, doi:10.1142/S0218202511005556*, 2011.